BACHELOR PROJECT:

SOLAR ENERGY POTENTIAL IN NIGERIA

BY

STEFAN HROUDA-RASMUSSEN | SHRO@ITU.DK

SUPERVISOR

THERESE GRAVERSEN | THEG@ITU.DK

IT UNIVERSITY OF COPENHAGEN

6TH SEMESTER, SPRING 2020

DATA SCIENCE

COURSE CODE: BIBAPRO1PE

Abstract

Nigeria is the most populous country in Africa and has been facing electricity deficits for decades, despite being rich in resources. Reasons for this are often attributed to poor policy decisions and inadequate utilisation of resources. In this project I estimate access to electricity and the solar energy budget of Nigeria, as to propose a solar photovoltaic energy expansion plan. The results of these are combined to find areas of Nigeria, where allocation of electricity generation resources ensures the most people get access to electricity for the lowest capital investment. The project can be reproduced in other developing countries and aims to aid policy decision makers and funders make the best choices. All code is available at: https://github.itu.dk/shro/bachelor_project.

Contents

1 Introduction

In 2015, the United Nations General Assembly wrote 17 global goals into the UN Resolution 70/1 to be achieved by the year 2030, known as the Sustainable Development Goals (SDGs) (General Assembly, 2015). The seventh goal is to *"ensure universal access to affordable, reliable and modern energy services"* of which two indicators are used to measure the progress of this goal: Proportion of population with access to electricity and proportion of population with primary reliance on clean fuels and technology. The most recent figures from the Energy Progress Report[1] say, the proportion of the world population without access to electricity decreased from 17.3% to 11.2% between 2010 and 2017, and 42.8% without access to clean cooking fell to 38.6% (IEA et al., 2019). Yet, successful electrification efforts have been uneven across regions, with Asia and South America having made most of the progress, and sub-Saharan Africa retaining the largest deficit. IEA et al. (2019) estimated that this trend will continue; 573 of the 840 million people without access to electricity in 2017 were located in sub-Saharan Africa with a projected 585 out of 650 million in 2030. Hence, sub-Saharan Africa will far from reach the SDG by 2030.

The detriments of electricity deficit have been extensively discussed and substantiated (Sovacool, 2012; Cabraal et al., 2005), including, but not limited to, diminished care provision from health facilities (Herrin, 1979; Adair-Rohani et al., 2013), less gender equality and employment opportunities (Dinkelman, 2011; IEA et al., 2019), and lower literacy rates (Kanagawa and Nakata, 2008), which subsequently hampers the progress of the other SDGs.

One of the sub-Saharan countries that have been experiencing large electricity deficits for decades is Nigeria (Kennedy-Darling et al., 2008), despite possessing some of the world's largest oil and natural gas reserves (OPEC, 2019; BP, 2019). Figure 1 shows the proportions (and populations) of urban and rural populations with access to electricity, which reveal a notable disparity between them that has existed for decades. This disparity could be due to Nigeria's electrical grid, which doesn't extend to rural areas. However, even in urban areas, where most of the population is connected to the grid, erratic supply is common. Recent polls by NOIPolls, a partner of Gallup in Western Africa, indicate that citizens with access to electricity receive on average just under 10 hours of cumulative supply per day[2].

[1] An annual multi-agency publication by International Energy Agency (IEA), the International Renewable Energy Agency (IRENA), United Nations Statistics Division (UNSD), the World Bank, and the World Health Organization (WHO).

[2] NOIPolls: https://noi-polls.com/power-tracking-poll/

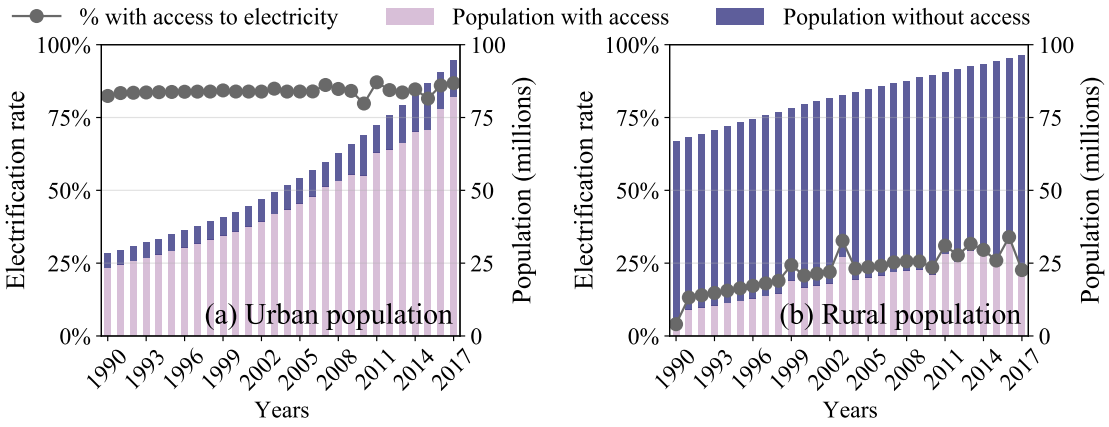

Figure 1: Populations in urban and rural areas of Nigeria and proportions with electricity. Data from the World Bank.

While the primary reasons for Nigeria's electricity deficit are contested, most research point to inadequate utilisation of resources, poor policy decisions, and corruption (Aliyu et al., 2013; Oyedepo, 2012), which has sprouted research into energy expansion planning. Global shifts towards renewable energy sources, due to the shortness of fossil fuels and urgency of limiting greenhouse gas emissions, sway these expansion plans toward suggesting solar-, wind-, and hydropower as the most likely sustainable candidates (Oyedepo, 2012). Especially solar power looks promising, as it accommodates the United Nations' prospect of clean technology, prices of solar panels have fortuitously been declining for decades (Farmer and Lafond, 2016; Swanson, 2006), and it is a suitable source of decentralized electricity for rural populations, since it's not reliant on the existing grid infrastructure.

To address the endemic electricity deficit, this project utilizes freely available satellite and survey data to analyze the off-grid and decentralized solar photovoltaic energy potential in Nigeria by estimating optimal initial locations for installing solar power plants. This is to ensure allocation of electricity generation resources can be deployed in areas, where the highest cost-benefit can be reached ensuring the most people get access to electricity for the lowest capital investment.

Two distinct subproblems are defined and examined; firstly, finding areas with a need of electricity, and secondly, estimating the solar energy budget. These two problems will henceforth be referred to as the "electricity deficit" and "solar budget" part of the project. For the deficit, freely available household survey and satellite data are used in a geostatistical approach, following the methodology of Andrade-Pacheco et al. (2019), to estimate electricity access in Nigeria. Access to electricity in Nigeria is predicted for 2019 and mapped with a

1 km resolution. For the budget, freely available satellite data are gathered and curated, and a programmatic tool to estimate solar irradiation, following the model by Bird and Hulstrom (1981), is constructed. The estimates are performed at 3-hourly intervals from 2003 to 2018 to build a picture of the microclimate, and thereafter a typical meteorological year of solar irradiance in Nigeria is mapped. Finally, the results are analyzed in unison to come up with a proposal of optimal initial locations for solar photovoltaic energy expansion in Nigeria. All code is available at: `https://github.itu.dk/shro/bachelor_project`.

2 Electricity deficit: Estimating access to electricity

Accurate data on electricity access is essential to policy decisions and infrastructure planning. However, due to the difficulties of monitoring electrification development through surveys, research has sought to estimate electricity access with spatial and spatio-temporal data (Falchetta et al., 2019). This is also due to the increased availability of spatial and spatio-temporal data by remote sensing applications. Concomitantly, geostatistical modeling has become more popular as well (Marta Blangiardo, 2015). Especially Bayesian methods have found their way into geostatistics with the development of Markov Chain Monte Carlo (MCMC) methods (Marta Blangiardo, 2015). However, accounting for the complexity of very large spatial and spatio-temporal datasets require significant computing time due to the computational burden of MCMC methods (Marta Blangiardo, 2015). Instead, the recently developed Integrated Nested Laplace Approximation (INLA) approach is a computationally efficient alternative to MCMC methods designed for latent Gaussian models (Marta Blangiardo, 2015). INLA uses numerical algorithms and analytical approximations to approximate closed-form expressions of the posterior distributions. For this project, the R-INLA package is used.[3].

Andrade-Pacheco et al. (2019) used spatial data from 2000 to 2013 to calculate values of the covariates used in the geostatistical model. However, this project focuses on the period from 2013 to 2018 to include more recent surveys conducted in Nigeria. Some of the sources of spatial data used in this project differs from Andrade-Pacheco et al. (2019), which is explained in Section 2.1. After which the model itself is described in Section 2.2, which follows the approach of Andrade-Pacheco et al. (2019). The result is shown in Section 2.3.

[3]R-INLA website: http://www.r-inla.org/

2.1 Data sources and preprocessing

2.1.1 Access to electricity

The Demographic and Health Surveys (DHS) program was established in 1984 to provide technical assistance with conducting surveys in developing countries, mainly to aid understanding of health and population trends (Trevor N. Croft, 2018). For participating countries, access to electricity (variable `hv206`), among other household indicators, are collected (Trevor N. Croft, 2018). To ensure data privacy, the surveyed households are aggregated into clusters, and only the locations of the cluster centroids are reported after being randomly displaced up to 2 km for urban areas and 5 km (with 1% displaced up to 10 km) for rural areas (Trevor N. Croft, 2018).

Andrade-Pacheco et al. (2019) used surveys from 2000 to 2013. In this project, however, of the eight surveys conducted in Nigeria between 1990 and 2018, three of them lie within the period covered by this part of the project (2013-2019). Clusters with reference location outside the boundary of Nigeria are disregarded. Summary statistics of these surveys are listed in Table 1.

Year	Clusters	Avg. # households per cluster	Avg. electrification rate per cluster
2013	889	43	0.55
2015	332	24	0.56
2018	1359	29	0.56

Table 1: Summary of the surveys conducted in Nigeria by the DHS program within the period studied in this project. Data is from the DHS program.

2.1.2 Nighttime lights

Global nighttime lights (NTL) imagery have become a popular geospatial data product (Falchi et al., 2016; Small et al., 2005; Sutton et al., 2001), and have previously been used to estimate electrification (Min et al., 2013; Amaral et al., 2005). The NTL imagery from the Defense Meteorological Satellite Program (DMSP) has been the standard, however, due to lack of intra- and intercalibration of satellites, the imagery is not directly applicable (Andrade-Pacheco et al., 2019). Post-calibrated DSMP NTL data was used by Andrade-Pacheco et al. (2019), which covers Africa from 2000 to 2013 (Savory et al., 2017). Yet, this does not fit the period studied in this project. Instead, I use the Visible Infrared Imaging Radiometer

Suite (VIIRS) NTL data, which are monthly composited NTL data ranging from April 2012 to present time (Elvidge et al., 2017).

The VIIRS data are freely availabe in GeoTIFF of monthly means through the Google Earth Engine upon registration[4]. Due to limited size transaction from the Earth Engine, the monthly composites are gathered in pieces of the highest available resolution, merged, and subsequently cropped to only contain Nigeria. Furthermore, to represent the NTL of an entire year, the monthly composites are averaged - the preprocessed result for 2015 is shown in Figure 2.

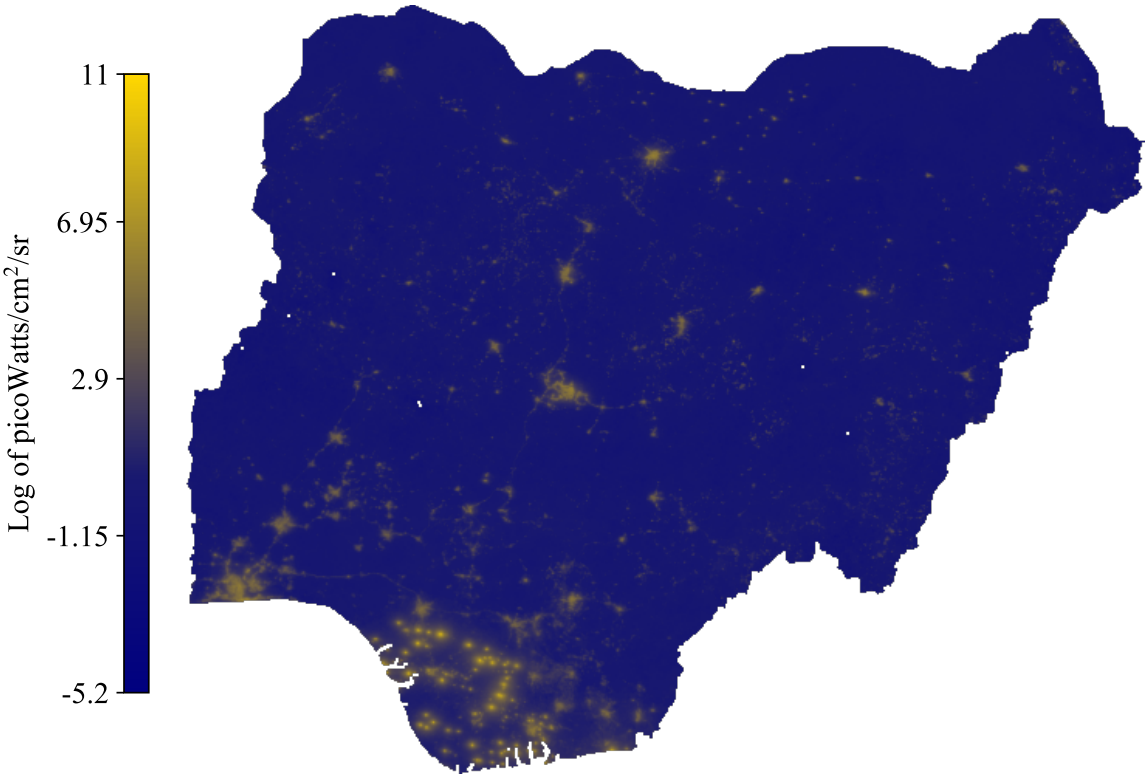

Figure 2: Average of VIIRS nighttime light monthly composites of 2015 in Nigeria. Due to very few bright lights, the log of the values are illustrated. Data from Google Earth Engine.

2.1.3 Population distribution

The WorldPop program was initiated in 2013 and combined the continent-specific programs AfriPop, AsiaPop, and AmeriPop, to produce high-resolution maps of population distributions[5]. The maps are created with a dasymetric modeling approach using random forests with

[4]Earth Engine VIIRS dataset: https://developers.google.com/earth-engine/datasets/catalog/NOAA_VIIRS_DNB_MONTHLY_V1_VCMCFG

[5]WorldPop website: https://www.worldpop.org/about

various geospatial datasets as inputs, and are availabe for all years between 2000 and 2020 in about a 100 meters resolution (Stevens et al., 2015). Individual countries are available in GeoTiff, thus no preprocessing is required. The map of the Nigerian population distribution in 2015 from WorldPop can be seen in Figure 3.

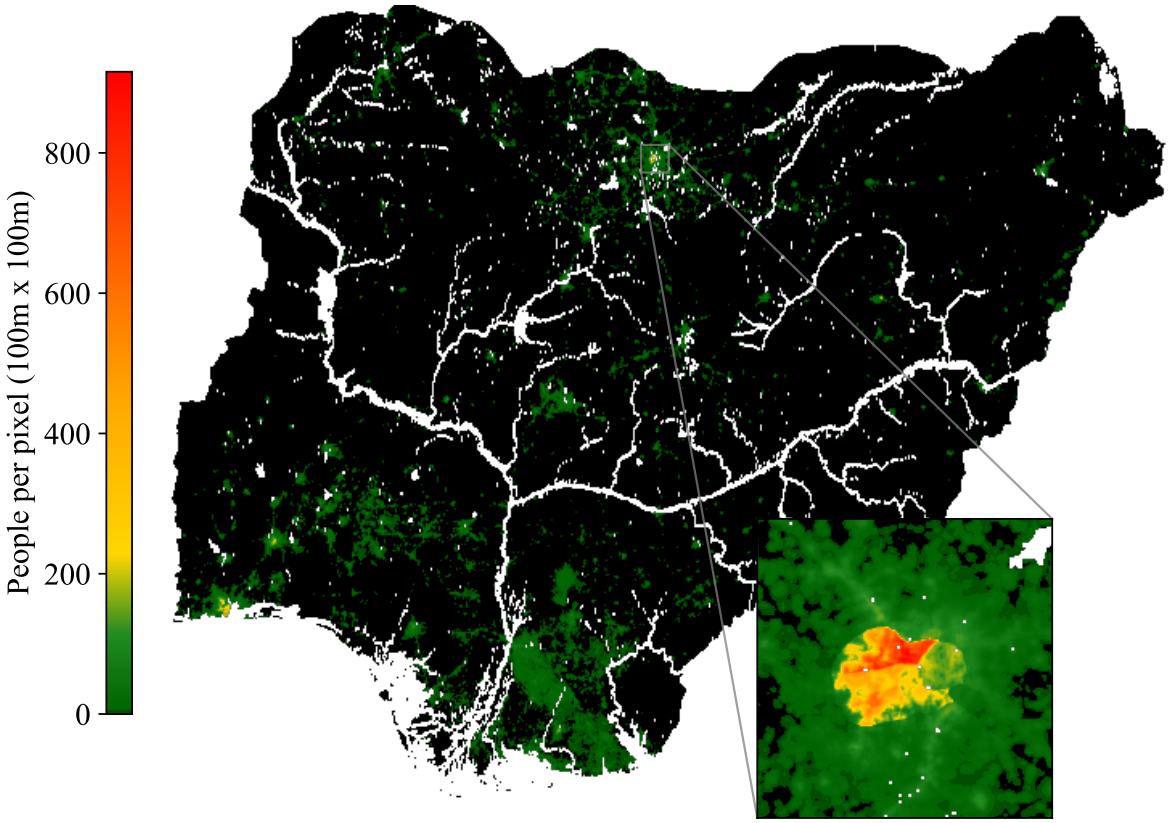

Figure 3: Map of the population distribution in Nigeria, 2015. Data from WorldPop.

2.1.4 Land use and land cover

Andrade-Pacheco et al. (2019) used Land Use and Land Cover (LULC) rasters using data from the NASA Landsat program (Midekisa et al., 2017). An important note is that the LULC rasters use the post-calibrated DSMP NTL data in their construction. The rasters consist of 7 categories: impervious surface, low biomass, high biomass, bare soil, sand, rock and water. The same data is used in this project.

Since Andrade-Pacheco et al. (2019) worked with a 5 km resolution, the LULC rasters were downscaled and two additional variables were constructed: impervious area proportion (IAP) and proximity to an impervious area (PIA). In this project, since I work on a much lower resolution, the LULC rasters are not downscaled and the IAP variable is not needed.

However, the PIA variable is constructed as the minimum Euclidean distance to an impervious area, as to signify distance to urban centers.

2.2 Formulation of geostatistical model

The geostatistical model used is from Andrade-Pacheco et al. (2019), where a generalized linear model with a spatial random effect and year included as a fixed effect was shown to have the best performance according to the conditional predictive ordinate. Instead of adding a spatiotemporal random effect, the year was included as a fixed effect due to the sparseness of data in time (Andrade-Pacheco et al., 2019). Let $\mathbf{x}_i \in \mathbb{R}^2$ specify the spatial reference point of the ith cluster (latitude, longitude). Given the true electrification rate $p(\mathbf{x}_i)$ for $i = 1, \ldots, N$, the model assumes that the number of households with access to electricity y_i in a cluster of n_i households follows a binomial distribution

$$y_i \mid p(\mathbf{x}_i) \sim \text{Binom}(n_i, p(\mathbf{x}_i)). \tag{1}$$

The logit of the electrification rate is then expressed as a sum of covariates and a spatial random field as

$$\text{logit}\left(p(\mathbf{x}_i)\right) = \sum_{j=1}^{7} \tau_{ij} + \sum_{j=1}^{3} \beta_j z_{[\mathbf{x}_{ij}]} + f_{\mathbf{x}_i}, \tag{2}$$

where τ_{ij} are fixed categorical covariates, z are the remaining covariates with corresponding regression parameters β_j, and $f_{\mathbf{x}_i}$ is a spatial random field that follows a zero-mean multivariate Gaussian process with Matérn covariance (Andrade-Pacheco et al., 2019).

Following the approach by Andrade-Pacheco et al. (2019) and suggestion by Trevor N. Croft (2018) the covariate values for NTL, PIA, and population are computed by taking the mean in a 5 km radius around the cluster locations, and the mode is used for LULC instead of the mean.

2.3 Map of electricity access

The probability of electricity access was predicted in Nigeria in 2019. The map of electricity access in 2019 is shown in Figure 4, and has a resolution of about 1 km.

To assess the performance of the model, I trained the model on the surveys conducted in 2013 and 2015 and then predictions were made on the survey conducted in 2018. The model

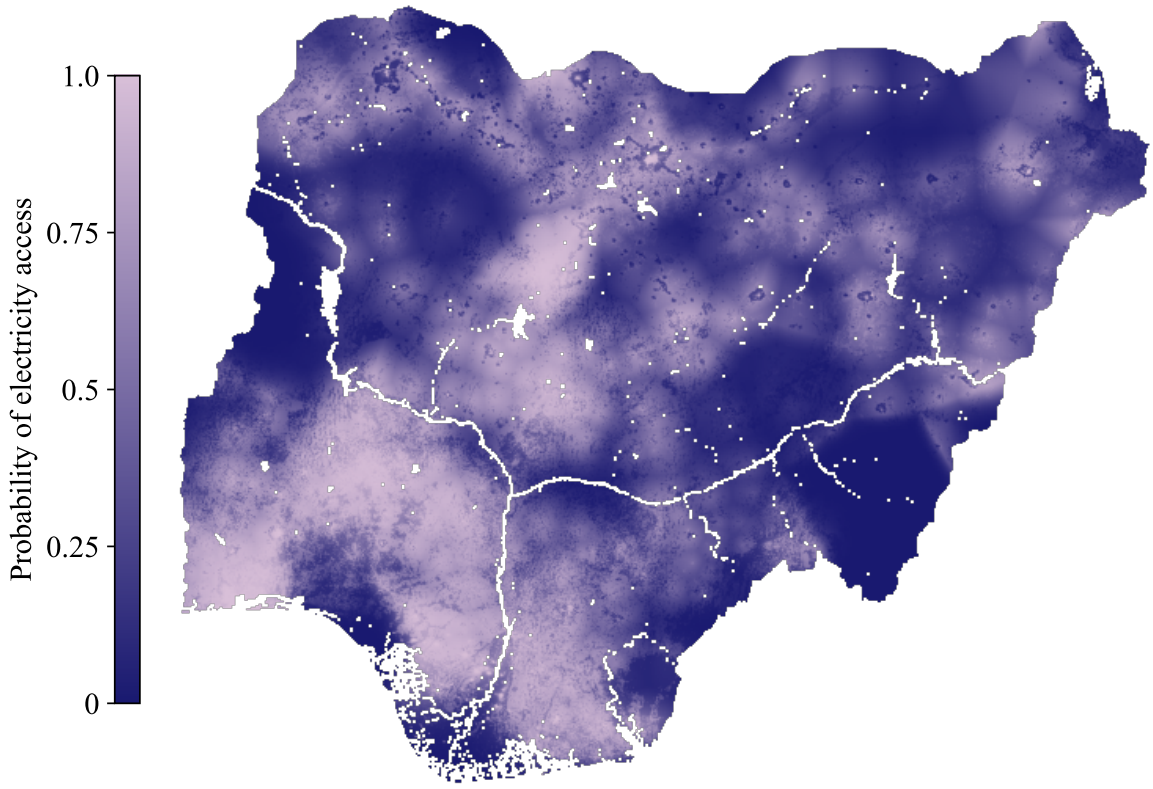

Figure 4: Probability estimates of electricity access in Nigeria, 2019. The resolution is about 1 km.

managed to correctly classify 74.8% of the cases from 2018. The precision and recall were 78.1% and 76.9% respectively when predicting households *with* electricity, and 70.6% and 72.0% when predicting households *without* electricity.

3 Solar budget: Estimating solar irradiance

Accurate solar irradiance data at a location can only be obtained through site measurement and is measured at weather stations. However, weather stations are sparse and with limited measuring devices in developing countries (Chineke et al., 1999). Perez et al. (1997) showed that while interpolated site measurements of solar irradiance is more accurate than satellite-derived estimates, this only holds up to 34 km from the sites. Instead, parameterization models (approximations of complex models in atmospheric modelling) using satellite data are used because of their accuracy, global reach, and the increase of available satellite data (Myers, 2017).

I begin with a description of the utilized satellite data, after which the solar irradiance estimate is formulated. A brief explanation of some of the programmatical details required

for the estimation follows, and finally, the solar budget, an average of solar irradiance from 2003 to 2018, is evaluated.

3.1 Data sources and preprocessing

3.1.1 Topography

A digital elevation model (DEM) is a three-dimensional representation of the topography of a terrain, and can be used to estimate station pressure, solar zenith angles, terrain shadows, etc. Copernicus (2017) evaluated commercial and freely available global DEMs. However, as the commercial DEMs were too expensive for this project, and the increased resolution would not have a significant impact on the project - three relevant freely available DEMs were assessed: SRTM-1[6], ASTER GDEM v2[7], and ALOS World 3D[8].

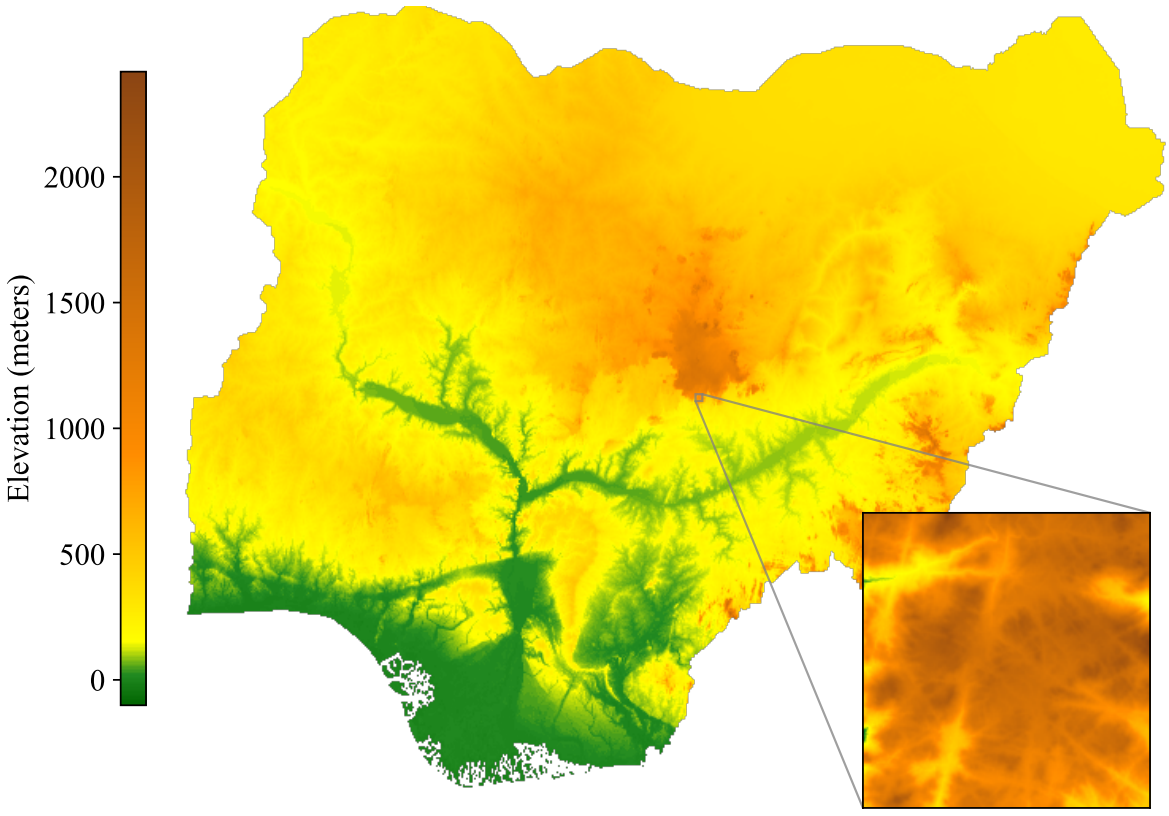

Figure 5: Digital elevation model (DEM) of the topography of Nigeria. A zoomed in area is also shown to illustrate the resolution. Data from the ALOS World 3D (AW3D30) Version 3.1.

Numerous factors influence the quality of DEMs, including, but not limited to, horizon-

[6]Shuttle Radar Topography Mission (SRTM): https://doi.org/10.5066/F7PR7TFT

[7]Advanced Spaceborne Thermal Emission and Reflection Radiometer (ASTER): https://asterweb.jpl.nasa.gov/gdem.asp

[8]Advanced Land Observing Satellite (ALOS): https://www.eorc.jaxa.jp/ALOS/en/aw3d30/index.htm

tal resolution, coverage, and vertical accuracy, which for this project are the three primary factors to consider. All three freely available DEMs have a horizontal resolution of about 1 arcsecond (approximately 30 meters) at the equator, and all of them have Nigeria included in their coverage (Copernicus, 2017). However, some tiles in SRTM may contain voids[6]. A few papers have compared the vertical accuracies of the three DEMs in different parts of the world with ALOS displaying the highest vertical accuracy (Florinsky et al., 2018; Santillan and Makinano-Santillan, 2016), and while vertical accuracy varies widely on the location, Yap et al. (2019) found that ALOS outperformed SRTM and ASTER in Cameroon neighbouring Nigeria. Hence, with the assumption that the terrains of Cameroon and Nigeria are similar because of their proximity, I will be using ALOS. Since the ALOS DEM is already in GeoTIFF, the preprocessing consists only of cropping it to contain Nigeria, resulting in a very fine 43230×34639 raster image of elevations. The DEM is shown in Figure 5 with a zoom to illustrate the resolution.

The ALOS was launched on January 24, 2006, equipped with three radiometers that took millions of stereoscopic images from 2006 to 2011 (Takaku et al., 2014; Tadono et al., 2014). These images were used to create the commercial "ALOS World 3D" with 5 meters horizontal resolution as well as the freely available version with 30 meters horizontal resolution (Takaku et al., 2014; Tadono et al., 2014).

3.1.2 Atmospheric composition

Data of the atmospheric composition is required to estimate the amount of solar radiation that is absorbed or scattered in the atmosphere. Acquiring the data from the same source with the same spatial and temporal resolution would ease preprocessing. The European Centre for Medium-Range Weather Forecasts (ECMWF) is an independent organization established in 1975, supported by more than 30 countries, possesses one of the largest supercomputer facilities in Europe[9], and known for their numerical weather predictions[10]. The Copernicus Atmosphere Monitoring Service (CAMS) reanalysis dataset[11] is a global reanalysis dataset of atmospheric composition in ongoing development by ECMWF, currently spanning from 2003 to 2018.

[9]ECMWF website: https://www.ecmwf.int/en/about/who-we-are

[10]Peter Bauer, Deputy Director of Research at ECMWF: https://www.earthmagazine.org/article/todays-weather-forecast-good-strong-chance-improvement

[11]CAMS reanalysis dataset: https://confluence.ecmwf.int/display/CKB/CAMS%3A+Reanalysis+data+documentation

The dataset has a spatial resolution of about 80 kms, and provide monthly means at 3-hourly steps of aerosol optical depth at 550nm, total column ozone, and total column water vapour at Earth's surface. Compared to the DEM, the resolution might seem extremely poor, but it does not get much better. These reanalysis dataset are created with numerical weather prediction models that require large supercomputers to compute.

The CAMS reanalysis dataset is one of the public datasets from the ECMWF[12] and requires only registration. Since the dataset is fetched in GRIB1 formats, preprocessing consists of converting it to GeoTIFF and cropping only to contain Nigeria. This provides 1536 coarse 18×14 raster images of measurements of 3 atmospheric components - an example for each hourly step of January 2010 is shown in Figure 6.

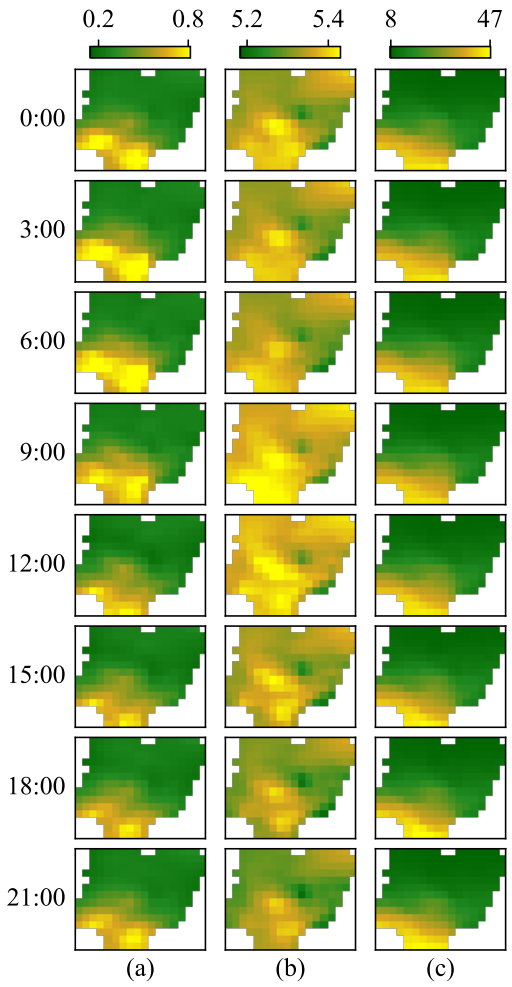

Figure 6: Monthly means at 3-hourly steps of (a) aerosol optical depth at 550nm, (b) total column ozone in $\frac{g}{m^2}$, and (c) total column water vapor in $\frac{kg}{m^2}$ in the atmosphere of January, 2010, above Nigeria. Data from the CAMS reanalysis dataset.

3.1.3 Cloud cover

Spectral imaging of the Earth provides information of the composition of the atmosphere and is frequently used in meteorology (Myers, 2017). Low altitude clouds are not considered aerosols in solar irradiance modeling but significantly impact modeling, as they can intercept more than 50% of the irradiation coming through the atmosphere (Myers, 2017). However, they are also the most turbulent (Myers, 2017), and hence to capture their impact, frequently updated images are required.

The Meteosat weather satellite series was initiated by the European Space Research Organization in 1972 with their first satellite launch (Meteosat-1) in November 1977[13]. The maintenance of the Meteosat program has since then been transferred to the European Organisation for the Exploitation of Meteorological Satellites (EUMETSAT); an intergovern-

[12]ECMWF public datasets: https://confluence.ecmwf.int/display/WEBAPI/Access+ECMWF+Public+Datasets
[13]Earth Observation portal: https://directory.eoportal.org/web/eoportal/satellite-missions/m/meteosat-first-generation

mental organization, supported by 30 EU member states, maintaining European meteorological satellites and processing meteorological data for weather forecasting[14]. Meteosat-8 and Meteosat-11 are the current primary geostationary weather satellites over Europe, Africa, and the Indian Ocean, capturing full disc images of Earth in 12 spectral bands every 15 minutes[15]. The nadir of Meteosat-11 is located at 0° longitude and 0° latitude, just outside the coast of Nigeria, making its images minimally distorted and thereby perfect for cloud detection in this project.

All data produced by the Meteosat series are free but not easily available. The data is broadcasted over radio waves in real-time, which requires a specific antenna to capture. EUMETSAT also has an online data delivery service that only requires registration[16], but with size limitations and significant delivery time, which wasn't sufficient for this project. Luckily, The University of Wisconsin-Madison Space Science and Engineering Center (SSEC) has a large archive of geostationary satellite data (including data from Meteosat) with a client-agnostic data retrieval method called McFetch[17] that also only requires registration. A few limitations are imposed on users, however, including up to 1000 transactions and 1 GB of data per day. Using McFetch, it was possible to acquire the necessary data for this project in 47 days.

The data from McFetch is in GeoTIFF and was cropped to contain only Nigeria, resulting in 46720 raster images of size 446×357 (an example is illustrated later on in (a) of Figure 7). It should be noted that there are a few weekly gaps in the data from Meteosat due to decontamination periods[18]. These gaps are removed and do not contribute to the project.

3.2 Formulation of solar irradiance at Earth's surface E

A common method of estimating solar irradiance at Earth's surface is first to calculate the amount of solar irradiance available *without* accounting for low-altitude clouds, called the clear-sky irradiance, and thereafter estimate the amount lost to clouds represented by the cloud index β (Myers, 2017).

[14]EUMETSAT website: https://www.eumetsat.int/website/home/AboutUs/WhoWeAre/index.html
[15]Meteosat Second Generation: https://www.eumetsat.int/website/home/Satellites/CurrentSatellites/Meteosat/index.html
[16]EUMETSAT Data Centre: https://www.eumetsat.int/website/home/Data/DataDelivery/EUMETSATDataCentre/
[17]McFetch: https://mcfetch.ssec.wisc.edu/
[18]Meteosat product disruption: https://www.cmsaf.eu/EN/Products/KnownProductDisruptions/2005-2015/2005-2015_node.html

Let E denote the solar irradiance incident on the plane of the solar array on Earth's surface in cloudy conditions. The relation between E and the cloud index β is

$$E = (1 - \beta)E_{\text{POA}}, \tag{3}$$

where E_{POA} is called the plane-of-array (POA) irradiance, which is the clear-sky irradiance incident on the plane of the solar array. To estimate E_{POA}, it's necessary to know the irradiance available to Earth. The total solar irradiance (TSI) is the irradiance incident on a plane normal to the sunlight at the top of Earth's atmosphere. Because of the eccentricity in Earth's orbit around the Sun, TSI fluctuates slightly throughout the year. The TSI is estimated as

$$\text{TSI} = G_{\text{SC}} R_c, \tag{4}$$

where G_{SC} is the mean TSI, called the solar constant, and R_c is the Earth-Sun radius correction term at a given day of the year to account for the eccentricity. The value of the solar constant is about 1361 W/m^2 with an uncertainty of $\pm$ 0.5 W/m^2 (Kopp and Lean, 2011; Gueymard, 2018), and I'll use the formula derived by Spencer (1971) to estimate R_c.

Plane-of-array (POA) irradiance E_{POA}. The POA irradiance can be dissected into three parts

$$E_{\text{POA}} = E_b + E_d + E_g, \tag{5}$$

where E_b is the amount of direct normal irradiance (DNI) incident on the array, E_d is the radiation at the surface of the Earth scattered by the atmosphere, commonly called the diffuse horizontal irradiance (DHI), and E_g is the irradiance reflected off the ground incident on the array (Myers, 2017). Let θ_{AOI} denote the angle of incidence between the POA and the sunlight, i.e. the angle between the beam of sunlight and the plane of the solar array, we can then say

$$E_b = \text{DNI} \cos\left(\theta_{\text{AOI}}\right). \tag{6}$$

Let θ_z, θ_a denote the solar zenith and azimuth angles respectively, and let ϕ_t, ϕ_a denote the solar array tilt and azimuth angles respectively. The angle of incidence θ_{AOI} is then (Myers, 2017)

$$\theta_{\text{AOI}} = \cos^{-1}\left(\cos(\theta_z)\cos(\phi_t) + \sin(\theta_z)\sin(\phi_t)\cos(\theta_a - \phi_a)\right). \tag{7}$$

Direct normal irradiance (DNI). The atmosphere is composed of particles that either absorb or scatter certain wavelengths of the sunlight (Myers, 2017). The amount reaching a plane normal to the beam of sunlight is called the direct normal irradiance (DNI). Using the formulation of the DNI by Bird and Hulstrom (1981), we consider five different components that mitigate the sunlight, as it passes through the atmosphere: Rayleigh scattering by small particles, scattering and absorption by aerosols, absorption by ozone, absorption by water vapour, and absorption by less contributing gases (nitrogen, carbon dioxide, etc.). Bird and Hulstrom (1981) estimates the transmittance of each component to calculate the DNI as

$$\text{DNI} = \text{TSI}\, T_r T_a T_g T_o T_w, \tag{8}$$

where T_r is transmittance due to Rayleigh scattering, T_a is transmittance due to aerosols, T_g is transmittance due mixed gases, T_o is transmittance due to ozone, and T_w is transmittance due to water vapour. The transmittance equations require data from the atmospheric composition described in Section 3.1.2 and the pressure-corrected air mass M_p. The *geometric* air mass M is a relative measure of the path length through the atmosphere, where the shortest path is 1 (vertically through) (Myers, 2017). However, when the sun is not directly above the observer, the path length through the atmosphere is longer, which is accounted for by M defined as

$$M = \frac{1}{\sin(\pi - \theta_z)}. \tag{9}$$

As mentioned, Bird and Hulstrom (1981) use the pressure-corrected air mass M_p for the Rayleigh and mixed gas transmittance equations to account for the actual physical path length of the sunlight through the atmosphere. This pressure-corrected air mass is a function of the station pressure, however, no data of station pressure were used in the project. Instead, the following estimate of M_p from the given air mass and elevation h was used (Myers, 2017)

$$M_p = \frac{M}{e^{0.000832h}}. \tag{10}$$

Diffuse horizontal irradiance (DHI) E_d. Some of the solar radiation that is scattered or possibly absorbed and reemitted by particles in the atmosphere still manages to reach the surface of the Earth (Myers, 2017). The amount of irradiance from this effect is called the diffuse horizontal irradiance (DHI), and is measured as the amount of irradiance scattered by

the atmosphere that reaches a horizontal plane on Earth. This can also be thought of as the irradiance received from all points in the sky excluding the Sun disk. Photovoltaic systems sort to simplified approximations of the scattering functions that model the uncollimated DHI rays (Myers, 2017). Bird and Hulstrom (1981) estimate the amount of sky diffuse radiation D_s as

$$D_s = 0.79\,\text{TSI}\,\cos\left(0.01745\theta_z\right) T_g T_o T_w T_{aa}, \tag{11}$$

where θ_z is the Solar zenith angle, and T_{aa} is aerosol absorptance defined as

$$T_{aa} = 1 - \frac{1 - M + M^{1.06}}{10(1 - T_a)}. \tag{12}$$

Note that Equation (11) is only the sky diffuse radiation, the radiation reaching a horizontal surface E_{hs} is

$$E_{hs} = D_s \frac{0.5(1 - T_r) + 0.85\left(1 - \frac{T_a}{T_{aa}}\right)}{1 - M + M^{1.02}}. \tag{13}$$

However, Bird and Hulstrom (1981) recognized that some amount of the radiation reaching Earth's surface is reflected off the ground into the atmosphere, and scattered by the particles in the atmosphere down to Earth's surface again. This reflected sky radiation R_s is determined by the relation between aerosol transmittance T_a and aerosol absorptance T_{aa}

$$R_s = 0.2185 - 0.15\frac{T_a}{T_{aa}}. \tag{14}$$

Finally, Bird and Hulstrom (1981) estimate the DHI as

$$E_d = \text{DHI} = \frac{\alpha R_s \text{DNI}\cos\theta_z + E_{hs}}{1 - \alpha R_s}, \tag{15}$$

where α is the surface albedo, which will be described below.

Ground-reflected irradiance E_g. Some amount of the irradiance reflected by the ground will directly reach the solar array without being scattered in the atmosphere again (Myers, 2017). Assuming the irradiation on the ground is uniform, and the ground-reflected radiation is isotropic, Ineichen et al. (1990) estimates E_g as

$$E_g = \left(\text{DNI}\cos\theta_z + E_d\right)\alpha\frac{1 - \cos\phi_t}{2}. \tag{16}$$

Cloud index β and albedo α. The albedo is a measure of the reflectance of a surface (Myers, 2017). The values of the surface albedo are naively estimated as the average values observed within the last 28 days using the Meteosat data described in Section 3.1.3. Subtracting the estimated albedo from Meteosat images gives the cloud cover as illustrated in Figure 7. Min-max normalizing the cloud cover gives the cloud index β, which is a value between 0 and 1 representing the proportion of irradiance that is reflected from low altitude clouds.

(a) Raw Meteosat-10 image of Nigeria taken March 3rd, 2014, at 12 UTC.

(b) Albedo over Nigeria calculated as an average of the last 28 days. Data from Meteosat-10.

(c) Cloud cover over Nigeria calculated as the original Meteosat-10 image subtracted the albedo.

Figure 7: Illustration of the cloud index calculation. Data from Meteosat-10.

Shadows. An additional mitigation of radiation not described by Bird and Hulstrom (1981) is nearby terrain obstructing the direct sunlight, eliminating the contribution of DNI to the clear-sky irradiance. Given the site elevation h, and the solar altitude $\pi - \theta_z$ angle, we can calculate the length of the shadow l_s cast by the site

$$l_s = \frac{h}{\tan\cos(\pi - \theta_z)}. \tag{17}$$

Following the direction of the solar azimuth angle, we can determine where the shadow lies and can locate potential sites covered by the shadow. Let $h_s(d)$ denote the site elevation distance d from the original site in the direction of the solar azimuth. If $h_s(d) < d\tan\cos(\pi - \theta_z)$, then the site is covered by the shadow, otherwise it's not and is casting its own shadow. The elevation data used in this project is described in Section 3.1.1.

Solar zenith θ_z and azimuth θ_a. Celestial mechanics dates back to the 17th century with the advent of Kepler's laws, but accurate knowledge of the orbits and positions of the major

celestial bodies in our solar system over an extended period of time is only a recent result of astronomy (Bretagnon and Francou, 1988). Yet, until Reda and Andreas (2004, 2007) published the Solar Position Algorithm (SPA), most solar position algorithms reported an uncertainty greater than $\pm 0.01^\circ$ in estimating the solar zenith and azimuth angles with a valid time span varying from 15 to 100 years. The SPA achieves significant improvements with uncertainties of $\pm 0.0003^\circ$ from the year -2000 to 6000, but is also computationally excessive for applications requiring numerous estimates (Reda and Andreas, 2004, 2007; Blanc and Wald, 2012). To remedy the excessive computation of the SPA, Blanc and Wald (2012) devised the Solar Geometry 2 (SG2) algorithm based on approximations of the equations of the SPA to decrease the number of operations. The SG2 algorithm achieves uncertainties of $\pm 0.0015^\circ$ between 1980 and 2030, which fits the time frame of the project, and manages to speed up calculations of solar positions 120 times compared to the SPA (Blanc and Wald, 2012).

3.3 Implementation

Of the data used, the highest spatial resolution is the ALOS raster (30 m), and the highest temporal resolution is the data from Meteosat (15 minutes), as is listed in Table 2. This results in at least 143 billion calculations per day, if the solar irradiance at every possible location at every possible time would be calculated. Note that this is a very conservative estimate of just one calculation per pixel per time step; the SG2 algorithm by Blanc and Wald (2012) requires 20 additions, 30 multiplications, and 23 direct or inverse trigonometric functions for each estimation of the solar zenith and azimuth angles. The amount of calculations per day makes calculating the typical meteorological year (TMY) with such high resolutions infeasible without access to a supercomputer. Hence, the temporal resolution is downsampled to every third hour, and the spatial resolution of the solar zenith and azimuth estimates are downsampled five times, i.e. every fifth pixel is used. Everything is implemented in Python but compiled with Numba[19]. This significantly speeds up the Python code and makes it comparable to C. Using all four cores of an i5-2500k processor[20] made each time step of the estimation take just over a minute. The entire 16 year period took about two weeks of computation.

[19]Numba: http://numba.pydata.org/

[20]Specifications of i5-2500k processor: https://ark.intel.com/content/www/us/en/ark/products/52210/intel-core-i5-2500k-processor-6m-cache-up-to-3-70-ghz.html

Inputs	Source	Approx. spatial resolution	Temporal resolution
Elevation	ALOS World 3D	30 m	N/A
Atmospheric optical depth	CAMS reanalysis	80 km	Monthly means at 3-hourly steps
Total column ozone	CAMS reanalysis	80 km	Monthly means at 3-hourly steps
Total column water vapour	CAMS reanalysis	80 km	Monthly means at 3-hourly steps
Cloud cover	Meteosat	3 km	15 minutes

Table 2: Overview of the input data used in the estimation of solar irradiation.

A correction is made to the SG2 algorithm by Blanc and Wald (2012), verified by the authors; in equation (31) of the paper, the constant multiplied by the modified universal Julian date is 6.3000388 but has to be 6.300388.

3.3.1 Shadows

Since the plane we are working with is a raster image of pixels, finding the areas covered in shadows is non-trivial. Equation (17) gives us the length of a shadow l_s cast by terrain at some elevation h given the solar position described by the zenith angle θ_z and the azimuth angle θ_a. Using l_s and θ_a we must determine which pixels are intersected by the shadow, and which of these pixels have an elevation lower than the shadow at that point. An algorithm, accustomed from Bresenham (1965), is used in which the iteration is stopped if the pixel's elevation is higher than the shadow.

3.4 Typical meteorological year (TMY)

In the years from 2003 to 2018, I estimated the solar irradiance in Nigeria at 3-hourly steps in a 30 meter resolution, which provides a picture of the microclimate. Averaging all these estimates gives us a TMY that represents the potential solar power in Nigeria. This is shown in Figure 8.

My request to the Nigerian Meteorological Agency (NiMet)[21] for solar irradiance records for this project was unfortunately denied. It is not certain whether there were no such records, or they just were not willing to share them. Nonetheless, no proper validation of the performance of the model can be assessed without solar irradiance records from weather stations in Nigeria. However, sunshine hours and temperature have previously been used to estimate solar irradiance in Nigeria (Akpabio and Etuk, 2003), and an attempt to show the correlation

[21] Nigerian Meteorological Agency (NiMet) website: https://www.nimet.gov.ng/

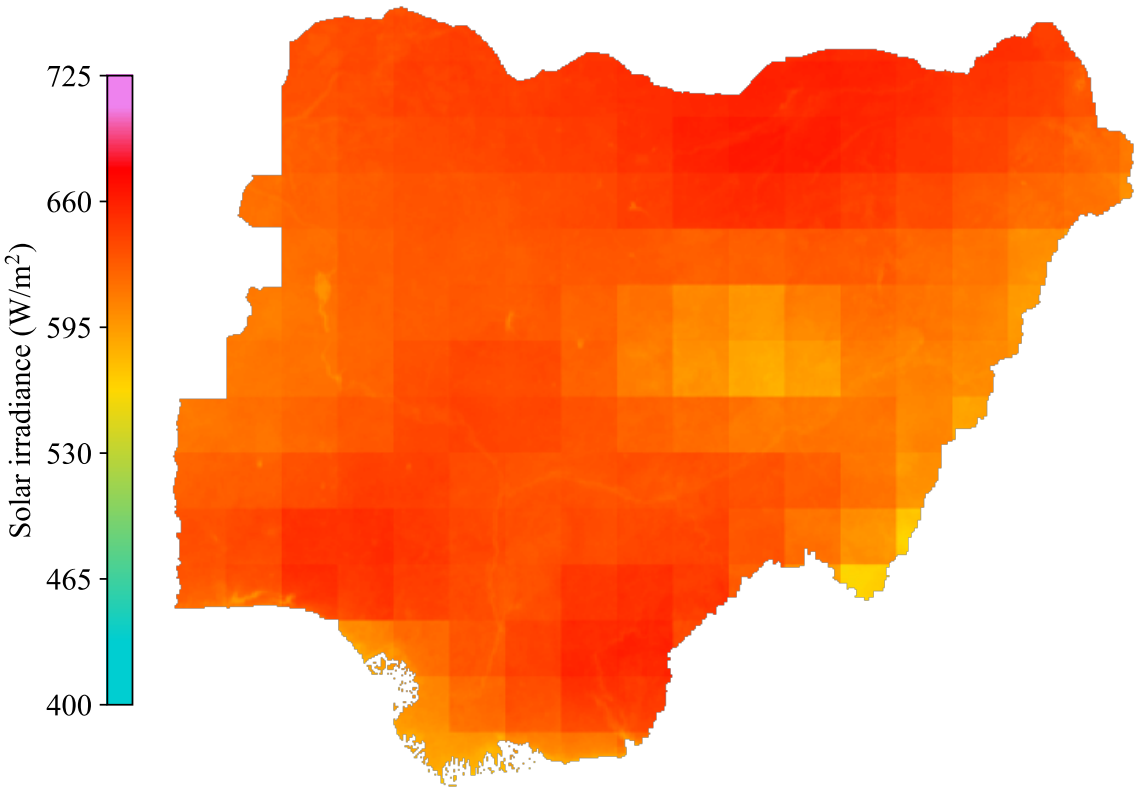

Figure 8: Typical meteorological year of solar irradiance in Nigeria from 2003 to 2018. The color scale is chosen to be comparable to Figure 9. Data and methodology used for creation is described in Section 3.1 and Section 3.2 respectively.

between the solar irradiance estimates and sunshine hour data from Manfred J. Muller (1982) was made. This analysis was left out of the project, but some results are shown in Section A.

Additionally, to show the variation throughout the year, the monthly averages of the solar irradiance estimates are shown in Figure 9. The low solar irradiance estimates of July and August coincide with the West African monsoon, and the high solar irradiance estimates in February, March, and April coincide with the West African dry season (Raj et al., 2019).

4 Discussion and error analysis

4.1 Electricity deficit

As a means of protecting the privacy of households, they are aggregated and the locations are randomly displaced, which is an inherent noise in the data that will affect any model. However, as shown by the sensitivity analysis of Andrade-Pacheco et al. (2019), the results with and without displacement are consistent.

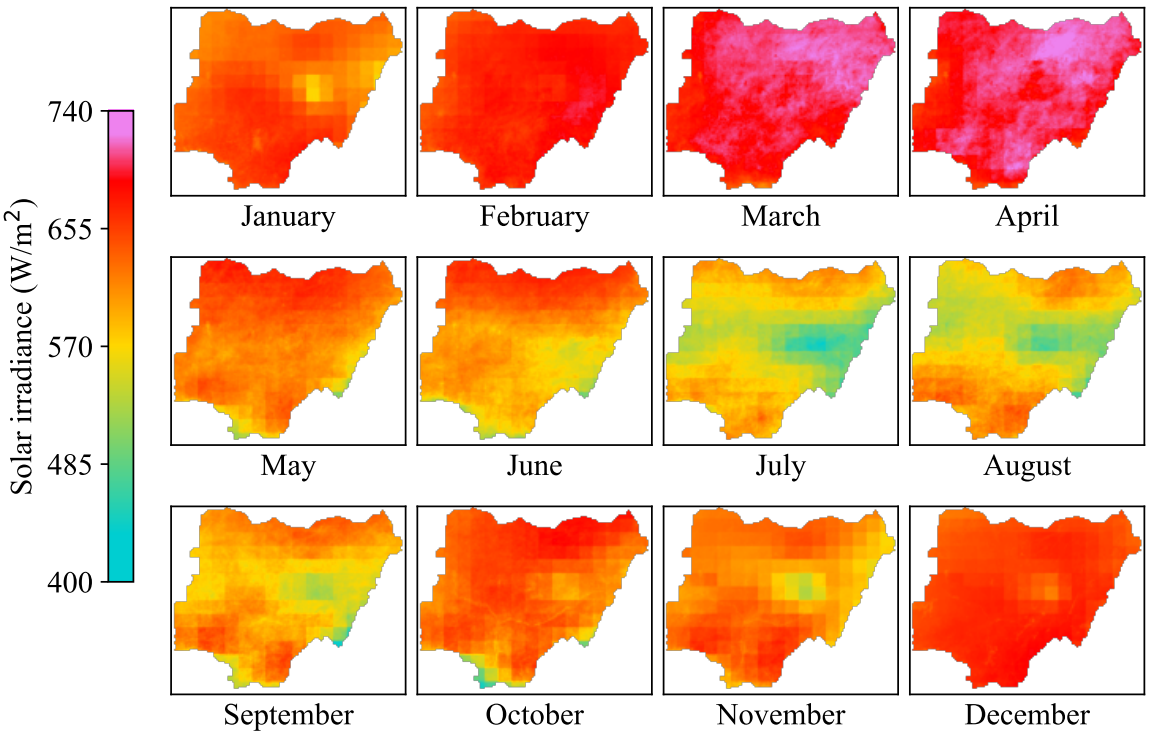

Figure 9: Monthly averages of solar irradiance in Nigeria from 2003 to 2018. Data and methodology used for creation is described in Section 3.1 and Section 3.2 respectively.

With the map of electricity access and the map of the Nigerian population distribution by WorldPop (see Section 2.1.3), we can estimate the number of people without access to electricity. This result is illustrated in Figure 10. However, the model has a tendency to overestimate the number of people with access to electrity; summing all the people in Figure 10 yields just over 43 million people, which only accounts for about half of the people without electricity access.

Comparing the distribution of the population without access to the overall distribution of the population (see Figure 3) reveals noticeably fewer dense clusters of people. This aligns with the disparity between urban and rural access to electricity (see Figure 1).

4.2 Solar budget

What is most notable in the TMY (see Figure 8) is the effect of the rasters of atmospheric compositions. However, this is to be expected as the main loss of solar irradiance in the model by Bird and Hulstrom (1981) is from the transmittances. Also, during computation an error in evaluating the exact location of pixels in the atmospheric composition rasters acted unexpectedly. The location, specifying a pixel, referred to the center of the pixel, which has

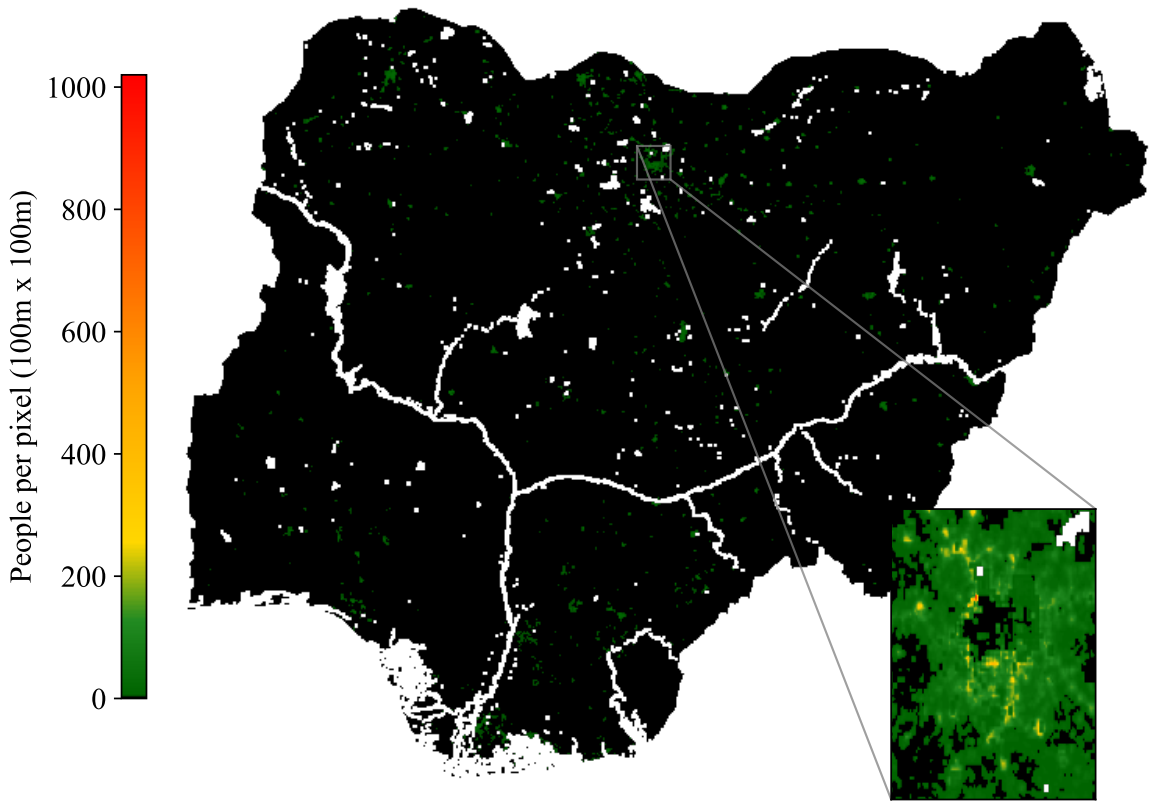

Figure 10: Map of the distribution of the population without access in Nigeria, 2019.

resulted in a few pixels in western Nigeria to be lost. This, however, has a small effect on the results.

The temporal resolution of three hours proved too short to properly estimate a day's worth of solar irradiance. A day would consist of only four estimates at 7:00, 10:00, 13:00, and 16:00 local time in Nigeria. However, the sun has barely risen at 7:00, which will lower the average.

4.3 Initial locations

An important note is that off-grid renewable energy sources is only part of the solution to Nigeria's electricity deficit. Grid infrastructure extension is often times a cheaper solution than investing in off-grid solutions, and making the choice between either is made on the number of households that would gain electricity per grid distance extension (Henry Louie, 2018). Furthermore, as mentioned in the beginning, erratic grid supply is common, and it's been estimated that up to 31 million Nigerians could be living under the grid without

connection[22], corresponding to about 40% of the population without access to electricity.

A recent collaboration between the World Bank and the open data science company Development Seed[23] used satellite images to map the current electrical grid in Nigeria. The data is freely available in a GeoJSON format[24]. Using this, we can find the people per distance to the grid for different communities - likewise, the inverse, distance to grid per person, would map the communities that are most economically viable candidates for off-grid solutions. Mahapatra and Dasappa (2012) further estimated that the economical distance limit for off-grid solar photovoltaic systems, i.e. the least distance from the existing grid infrastructure that off-grid solutions are economically favorable, is about 35 kms. Focusing our attention on communities more than 35 kms from the electrical grid and equally weighing the distance to grid per person against the solar budget, we can map the areas where most people get access to electricity for the lowest capital investment. Figure 11 (a) shows all areas that are suitable for solar photovoltaics, and Figure 11 (b) shows the optimal initial locations for a solar photovoltaic expansion plan in Nigeria. The areas in Figure 11 (a) account for just over 21 million people, and (b) account for 3.6 million.

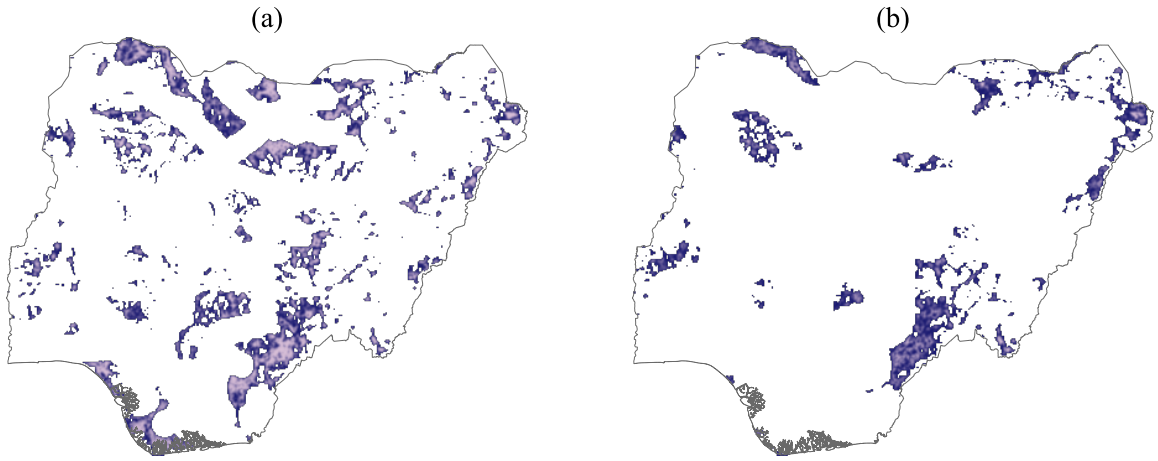

Figure 11: (a) shows all areas in Nigeria that are suitable for solar photovoltaics, and (b) shows the optimal initial locations for a solar photovoltaic expansion plan in Nigeria. These are generated from the methodology described in Section 2 and Section 3, including the map of the Nigerian electrical grid from the World Bank.

[22]Center for Global Development: https://www.cgdev.org/blog/living-under-grid-nigeria-new-estimates
[23]Development Seed website: https://developmentseed.org/
[24]Electrical grid in Nigeria: https://datacatalog.worldbank.org/dataset/nigeria-high-resolution-high-voltage-grid-map-based-machine-learning

5 Conclusive remarks

In this project, a solar power expansion plan to alleviate the endemic electricity deficit in Nigeria has been presented. The expansion plan targets areas where off-grid and decentralized solar photovoltaic energy potential in Nigeria is maximized. The areas are targeted mainly through the criteria of low access to electricity and high average yearly solar irradiance. Access to electricity was mapped using freely available satellite data and household surveys in a geostatistical approach, and a programmatic tool, not limited to Nigeria, was built to estimate solar irradiance also using freely available satellite data.

The methodology presented in this project can be reproduced in other developing countries. The information provided aims to aid funders and policy decision makers in making the best choices to provide electricity to the Nigerian population.

5.1 Future work

In regards to the solar budget, most importantly is acquiring site measurements of solar irradiance that can validate the estimates produced by the solar irradiance model. Expanding the examined area would achieve this, and since the underlying code is not limited to Nigeria, this would be a natural extension. However, this would also require substantial code optimization or larger computational power. With a proper method of validation, incremental improvements could be introduced to the model as well. Most notably is the current naive estimation of the cloud index, where using readily available albedo estimates could be used instead[25].

Examining a larger area is also a possibility with regards to the electricity deficit, as was originally done by Andrade-Pacheco et al. (2019). This might improve the ability of the model to relate the spatial effects. Obtaining spatial data from a longer time period to calculate the values of the covariates would make it possible to use surveys from before 2013.

[25] MODIS: https://modis.gsfc.nasa.gov/data/dataprod/mod43.php

References

Adair-Rohani, Heather, Karen Zukor, Sophie Bonjour, Susan Wilburn, Annette C Kuesel, Ryan Hebert, and Elaine R Fletcher. 2013. Limited electricity access in health facilities of sub-saharan africa: a systematic review of data on electricity access, sources, and reliability. *Global Health: Science and Practice*, 1(2):249–261.

Akpabio, Louis and Sunday Etuk. 2003. Relationship between global solar radiation and sunshine duration for onne, nigeria. *Turkish Journal of Physics*, 27:161–167.

Aliyu, Abubakar Sadiq, Ahmad Termizi Ramli, and Muneer Aziz Saleh. 2013. Nigeria electricity crisis: Power generation capacity expansion and environmental ramifications. *Energy*, 61:354 – 367.

Amaral, Silvana, Gilberto Câmara, Antônio Miguel Vieira Monteiro, José Alberto Quintanilha, and Christopher D. Elvidge. 2005. Estimating population and energy consumption in brazilian amazonia using dmsp night-time satellite data. *Computers, Environment and Urban Systems*, 29(2):179 – 195.

Andrade-Pacheco, Ricardo, David J. Savory, Alemayehu Midekisa, Peter W. Gething, Hugh J. W. Sturrock, and Adam Bennett. 2019. Household electricity access in Africa (2000–2013): Closing information gaps with model-based geostatistics. *PLOS ONE*, 14(5):1–14.

Bird, R. E. and R. L. Hulstrom. 1981. Simplified clear sky model for direct and diffuse insolation on horizontal surfaces.

Blanc, Ph. and L. Wald. 2012. The SG2 algorithm for a fast and accurate computation of the position of the Sun for multi-decadal time period. *Solar Energy*, 86(10):3072 – 3083.

BP. 2019. BP Statistical Review of World Energy.

Bresenham, Jack. 1965. Algorithm for computer control of a digital plotter. *IBM Syst. J.*, 4:25–30.

Bretagnon, P. and G. Francou. 1988. Planetary Theories in rectangular and spherical variables: VSOP87 solution. , 202:309.

Cabraal, Anil, Douglas Barnes, and Sachin Agarwal. 2005. Productive uses of energy for rural development. *Oct Annu. Rev. Environ. Resour*, 17:117–44.

Chineke, Theo, Ita Aina, and S Jagtap. 1999. Solar radiation data base for nigeria. *Discovery and Innovation*, 11.

Copernicus. 2017. Overview of Global DEM: Assessment of the current global DEMs and requirements for an updated global DEM.

Dinkelman, Taryn. 2011. The effects of rural electrification on employment: New evidence from south africa. *American Economic Review*, 101(7):3078–3108.

Elvidge, Christopher D, Kimberly Baugh, Mikhail Zhizhin, Feng Chi Hsu, and Tilottama Ghosh. 2017. Viirs night-time lights. *International Journal of Remote Sensing*, 38(21):5860–5879.

Falchetta, Giacomo, Shonali Pachauri, Simon Parkinson, and Edward Byers. 2019. A high-resolution gridded dataset to assess electrification in sub-Saharan Africa. *Scientific Data*.

Falchi, Fabio, Pierantonio Cinzano, Dan Duriscoe, Christopher C. M. Kyba, Christopher D. Elvidge, Kimberly Baugh, Boris A. Portnov, Nataliya A. Rybnikova, and Riccardo Furgoni. 2016. The new world atlas of artificial night sky brightness. *Science Advances*, 2(6).

Farmer, J. Doyne and François Lafond. 2016. How predictable is technological progress? *Research Policy*, 45(3):647 – 665.

Florinsky, I.V., T.N. Skrypitsyna, and O.S. Luschikova. 2018. Comparative accuracy of the AW3D30 DSM, ASTER GDEM, and SRTM1 DEM: A case study on the Zaoksky testing ground, Central European Russia. *Remote Sensing Letters*, 9(7):706–714.

General Assembly. 2015. Resolution 70/1.

Gueymard, Christian A. 2018. A reevaluation of the solar constant based on a 42-year total solar irradiance time series and a reconciliation of spaceborne observations. *Solar Energy*, 168:2 – 9. Advances in Solar Resource Assessment and Forecasting.

Henry Louie. 2018. *Off-Grid Electrical Systems in Developing Countries*.

Herrin, Alejandro N. 1979. Rural electrification and fertility change in the southern philippines. *Population and Development Review*, 5(1):61–86.

IEA, IRENA, UNSD, WB, and WHO. 2019. Tracking SDG 7: The Energy Progress Report 2019.

Ineichen, Pierre, Olivier Guisan, and Richard Perez. 1990. Ground-reflected radiation and albedo. *Solar Energy*, 44(4):207 – 214.

Kanagawa, Makoto and Toshihiko Nakata. 2008. Assessment of access to electricity and the socio-economic impacts in rural areas of developing countries. *Energy Policy*, 36(6):2016 – 2029.

Kennedy-Darling, Julia, Nick Hoyt, Kyle Murao, and Allison Ross. 2008. The Energy Crisis of Nigeria an Overview and Implications for the Future.

Kopp, Greg and Judith L. Lean. 2011. A new, lower value of total solar irradiance: Evidence and climate significance. *Geophysical Research Letters*, 38(1).

Mahapatra, Sadhan and S. Dasappa. 2012. Rural electrification: Optimising the choice between decentralised renewable energy sources and grid extension. *Energy for Sustainable Development*, 16(2):146 – 154.

Manfred J. Muller. 1982. *Selected climatic data for a global set of standard stations for vegetaion science*. Kluwer Academic Publishes Group.

Marta Blangiardo, Michela Cameletti. 2015. *Spatio and Spatio-temporal Bayesian Models with R-INLA*. John Wiley Sons, Ltd.

Midekisa, Alemayehu, Felix Holl, David J. Savory, Ricardo Andrade-Pacheco, Peter W. Gething, Adam Bennett, and Hugh J. W. Sturrock. 2017. Mapping land cover change over continental africa using landsat and google earth engine cloud computing. *PLOS ONE*, 12(9):1–15.

Min, Brian, Kwawu Mensan Gaba, Ousmane Fall Sarr, and Alassane Agalassou. 2013. Detection of rural electrification in africa using dmsp-ols night lights imagery. *International Journal of Remote Sensing*, 34(22):8118–8141.

Myers, D.R. 2017. *Solar radiation: Practical modeling for renewable energy applications*.

OPEC, Organization of the Petroleum Exporting Countries. 2019. OPEC Annual Statistical Bulletin.

Oyedepo, S.O. 2012. Energy and sustainable development in nigeria: the way forward. *Energy, Sustainability and Society*, 2(15).

Perez, Richard, Robert Seals, and Antoine Zelenka. 1997. Comparing satellite remote sensing and ground network measurements for the production of site/time specific irradiance data. *Solar Energy*, 60(2):89 – 96.

Raj, Jerry, Hamza Kunhu Bangalath, and Georgiy Stenchikov. 2019. West African Monsoon: current state and future projections in a high-resolution AGCM.

Reda, Ibrahim and Afshin Andreas. 2004. Solar position algorithm for solar radiation applications. *Solar Energy*, 76(5):577 – 589.

Reda, Ibrahim and Afshin Andreas. 2007. Corrigendum to "Solar position algorithm for solar radiation applications" [Solar Energy 76 (2004) 577–589]. *Solar Energy*, 81(6):838.

Santillan, Jojene and Meriam Makinano-Santillan. 2016. VERTICAL ACCURACY ASSESSMENT OF 30-M RESOLUTION ALOS, ASTER, AND SRTM GLOBAL DEMS OVER NORTHEASTERN MINDANAO, PHILIPPINES. *ISPRS - International Archives of the Photogrammetry, Remote Sensing and Spatial Information Sciences*, XLI-B4:149–156.

Savory, David J., Ricardo Andrade-Pacheco, Peter W. Gething, Alemayehu Midekisa, Adam Bennett, and Hugh J. W. Sturrock. 2017. Intercalibration and gaussian process modeling of nighttime lights imagery for measuring urbanization trends in africa 2000–2013. *Remote Sensing*, 9(7):713.

Small, Christopher, Francesca Pozzi, and C.D. Elvidge. 2005. Spatial analysis of global urban extent from dmsp-ols night lights. *Remote Sensing of Environment*, 96(3):277 – 291.

Sovacool, Benjamin K. 2012. The political economy of energy poverty: A review of key challenges. *Energy for Sustainable Development*, 16(3):272 – 282.

Spencer, J. W. 1971. Fourier series representation of the position of the sun. *Search*, 2(5):172+.

Stevens, Forrest R., Andrea E. Gaughan, Catherine Linard, and Andrew J. Tatem. 2015. Disaggregating census data for population mapping using random forests with remotely-sensed and ancillary data. *PLOS ONE*, 10(2):1–22.

Sutton, P., D. Roberts, C. Elvidge, and K. Baugh. 2001. Census from heaven: An estimate of the global human population using night-time satellite imagery. *International Journal of Remote Sensing*, 22(16):3061–3076.

Swanson, Richard M. 2006. A vision for crystalline silicon photovoltaics. *Progress in Photovoltaics: Research and Applications*, 14(5):443–453.

Tadono, Takeo, H. Ishida, F. Oda, S. Naito, K. Minakawa, and H. Iwamoto. 2014. Precise global DEM generation by ALOS PRISM. *ISPRS Annals of Photogrammetry, Remote Sensing and Spatial Information Sciences*, II-4.

Takaku, Junichi, Takeo Tadono, and K. Tsutsui. 2014. Generation of high resolution global dsm from alos prism. *ISPRS - International Archives of the Photogrammetry, Remote Sensing and Spatial Information Sciences*, XL-4.

Trevor N. Croft, Courtney K. Allen et al., Aileen M. J. Marshall. 2018. Guide to DHS Statistics.

Yap, Loudi, Ludovic Houetchak Kandé, Robert Nouayou, Joseph Kamguia, Nasser Abdou Ngouh, and Marie Brigitte Makuate. 2019. Vertical accuracy evaluation of freely available latest high-resolution (30m) global digital elevation models over Cameroon (Central Africa) with GPS/leveling ground control points. *International Journal of Digital Earth*, 12(5):500–524.